Independent design method of multiple surface modes using a domino-ring structure

Go Itami [*]

Sony Group Corporation, 1-7-1 Konan, Minato-ku, Tokyo 108-0075, Japan

This paper proposes a method for generating and independently controlling multiple modes of surface modes using a domino-ring structure. The domino structure, which forms a waveguide, gives a reference potential to the ring structure to realize a waveguide in which multiple surface modes are formed. The two-dimensional periodic structure of the ring mimics the helical edge state, one of the characteristic properties of topological materials, and the number of modes is independent of the shape. The quasi-two-dimensional periodic structure obtained by stacking the ring structure and combining it with the domino structure multiplexes the surface modes and produces coupling modes as the complimentary modes. Eigenvalue analyses are performed to calculate the dispersion relations for the domino, ring, and domino-ring structures, and the results were compared with the theoretical curve for the domino structure and the fitting curve for the ring structure, and the mode controllability and skin depth of the modes are discussed. The results show good agreement between the theoretical and fitting curves and the analytical results and also confirmed that the modes are generated according to the number of rings in the unit cell. And it confirmed that the skin depth of the multiple surface modes on the domino-ring structure varies with each coupling point and can be controlled by the exciting condition.

I. INTRODUCTION

Surface waves are unique electromagnetic modes that form at the boundary of a medium and propagate within the boundary due to oscillations caused by compressional waves. Surface plasmon polaritons (SPPs) are better known as surface wave modes excited by light waves [1–11]. Gold, silver, and platinum are the main materials known as conductors that can excite SPPs [1–3]. The basic principle of SPP excitation is that the excitation wavelength is determined by the material properties and the angle of incidence. There are two excitation methods using a conductor plate and prism: the Kretschmann configuration and the Otto configuration [1,4,5]. There is also a method of excitation without using a prism by applying a periodic structure to the conductor [2]. SPPs have important features such as field concentration effects and resolution beyond the diffraction limit, and have been used in combination with scanning near-field optical microscopy and other techniques, mainly in chemical and biosensing applications [6–10].

A similar phenomenon of electromagnetic field mode formation in the frequency bands lower than the optical frequency band has been discovered and is called spoof surface plasmon polariton (SSPP). This phenomenon was discovered by Pendry in 2004, and is known that surface wave-like electric field distributions are formed on a conductive periodic structure [12]. As well as SPPs, the extraordinary transmission (EOT) phenomenon, showing energy transmission over the aperture ratio is also known as a characteristic property of SSPP [11,13–15]. SSPP structures are classified as one of metamaterials in the broad sense, since it can be used to control the wave modes [11,12,16–19]. SSPPs have been applied to spatial filters, high-frequency transmission lines, and antennas, and are mainly used for sensing [20–23].

From the viewpoint of condensed matter physics in surface modes, topological materials have attracted much attention in recent years [24–30]. The quantum Hall effect was first observed in two-dimensional systems and was later extended to three-dimensional systems [24]. One of the characteristics of topological materials is that they exhibit dielectric properties in the bulk region while exhibiting a metallic state at the surface. This metallic state is due to topological order and is known to be resistant to structural perturbations, unlike ordinary surface states. This feature has the same meaning as the topological distinction between donuts and balls by the number of holes.

When considering engineering applications, surface wave structures are mainly expected to be used for sensing, the focus has been on improving sensitivity and spatial resolution and controlling skin depth [31–33]. For the enhancement of sensitivity and spatial resolution, improvement of sensor structure and multimode generation by thin-film technologies have been studied [31,32]. In the area of skin depth engineering in the optical bands, studies on suppressing light seepage in fibers and reducing transmission loss have been reported [33]. On the other hand, in the terahertz region, the relationship between the skin depth and the structure of the SSPP structure has been studied theoretically, analytically, and experimentally, and the possibility of medical applications is also being considered [34–38]. In recent years, however, millimeter-wave and terahertz-wave applications have become popular not only for sensing but also for wireless communications, and there is an increasing number of scenarios where both technologies are required simultaneously [39,40]. For example, in automatic driving, information obtained by radar can be shared with surrounding vehicles in real time via millimeter-wave communications. In such

*Go.Itami@sony.com

applications, it is important not only to expand bandwidth, but also to use multiple individual bandwidths.

There are two main approaches to multiple-modes surface wave generator structures. One is to use only propagating plasmons and design the periodic structure to generate multiple modes, such as multiple-modes transmission lines and harmonic generation waveguides [41,42]. The other is to combine localized plasmons and propagating plasmons, in which both are excited simultaneously [32,43]. In this method, particles that excite localized plasmon are stacked three dimensionally to form a periodic structure that excites propagating plasmon. Here for example, localized plasmon particles refer to those of gold and silver. When only propagating plasmons are used, although multimode transmission lines can be applicable for increasing the number of propagation modes by separating ports, the number of modes corresponding to a single port cannot be increased to multiple modes [41]. In the conventional method the number of modes depends directly on the type of unit cell in the transmission line, and this can complicate the design by changing the length of the transmission line and the combination of unit cells. As similar techniques, there are examples of using harmonic modes, but the strong correlation between modes makes it impossible to design each mode independently [42]. In the case of combining localized plasmon and propagating plasmon, there are two possible methods: one is to design multiple types of particles that excite localized plasmons for creating multiple modes, and the other is to form multiple modes by arranging periodic structures composed of particles. In the former method, there is a concern that the particle diameter may change depending on the mode, making the design difficult [32]. In the latter case, as in the case of multiple-modes transmission lines, the length of the transmission line and the combination of the unit cells may change, complicating the design [43]. As discussed above, the essential difficulty of multiple-modes design originates from the design of boundary conditions based on wave theorem. It is geometrically difficult to superimpose aperture-type structures that serve as reference potentials in parallel. On the other hand, when designing a resonant circuit based on circuit theory, it is difficult to set a reference potential, and waves on each resonator are reradiated without propagating along the structure.

In this paper, a method for designing independent multiple modes of surface waves is proposed. The method is based on the combination of a domino structure, which is a typical structure for generating surface waves, and multiple ring structures. The domino structure, which forms a waveguide, gives a reference potential such as ground/GND to the ring structures to realize a waveguide in which multiple modes are formed. The two-dimensional periodic structure of the ring also has the properties of a topological material and is considered to simulate a helical edge state when assuming a finite array in a vertically canceling static magnetic field. Stacking this two-dimensional system in combination with a domino structure allows the bulk to be multiplexed as a propagating surface mode. And multilayered two-dimensional systems simultaneously create complementary spaces, which form coupling modes. This is consistent with the shape-independent nature of the number of surface modes corresponding to Chern number [30].

The modes generated by the domino and the ring structures are determined by each structure, and can be controlled by structural parameters such as size, position, and period of the structure. The proposed design enables simpler, more controllable, and more accurate design of multiple surface modes compared to the conventional methods. First, the proposed surface wave structure with domino and multiple-ring structures and the operating principles of surface wave generation are described. Next, generation and control method of multiple surface modes using the proposed structure is discussed. Finally, it summarize the results obtained from the examinations as a conclusion.

II. OPERATING PRINCIPLE OF MULTIPLE SURFACE MODES

First, the design concept of the domino-ring structure is explained. The relationship between the two-dimensional periodic structure of the ring and topological materials is discussed. Assuming a finite array of rings, modes are generated and chiral edge states are formed as shown in Figs. 1(a) and 1(b) [26]. The static magnetic field and the corresponding electron motion (electric field) are divided into two patterns: clockwise and counterclockwise. This mimics the mode formation of edge magnetoplasmon, which is known to produce integer quantum Hall effect in the actual mode [30]. If there is no static magnetic field, the bidirectional static magnetic field can be regarded as canceling each other, resulting in a superposition of the two modes (helical edge state) due to time-reversal symmetry. The model remains consistent when generalized to include the case of infinite periodic arrays. This phenomenon is closed within a two-dimensional system, and is considered to be maintained even when N layers are stacked perpendicular to the two-dimensional periodic structure of the ring, as shown in Fig. 1(c). Therefore, the combination with the domino structure that produces surface modes makes it possible to form multiple surface modes. On the other hand, when combined with a domino structure, the complementary space formed between rings and dominos likewise creates a two-dimensional structure, and modes are formed in a manner corresponding to the number of rings. This is defined as a coupling mode. From the above discussion, the two-dimensional periodic structure of the ring has a number of modes (corresponding to Chern number) that is independent of the shape and simulates topological properties. The two-dimensional periodic structure of the rings acts as a wave source for the incident wave, transmitting and reflecting the wave, so that a propagation plane is not actually formed. This can be regarded as simulating the bulk state. Combined with the domino structure, a quasi two-dimensional surface is formed in which the multilayered structure of the ring surface is integrated, and multiple surface modes propagate. The proposed method of multiplexing surface modes is considered a reasonable design concept based on the above theory. On the other hand, the specific design of the multiple modes in this study can be more concisely understood by considering it as a combination of wave theory and circuit theory. In this study, the design concept of deriving the propagation mode by treating the conducting structure as a reference potential and solving the boundary conditions is called the wave theory. The design concept of deriving the propagation mode based on the current
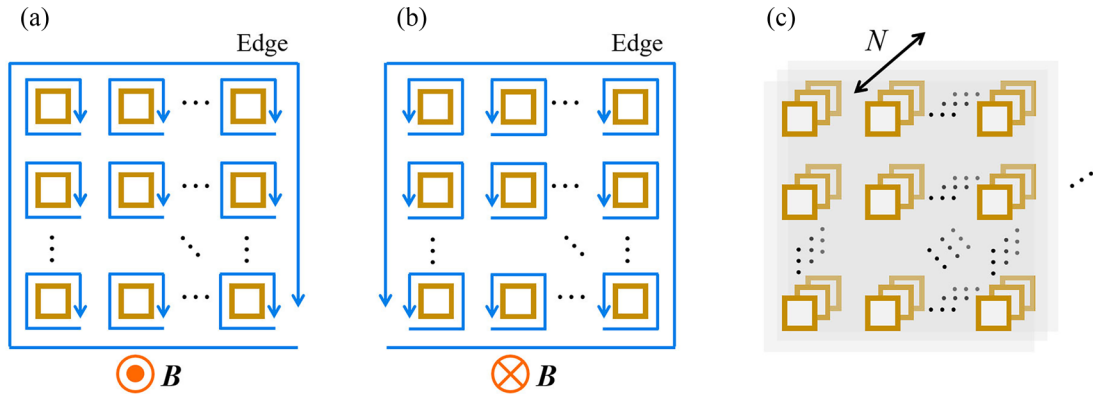
FIG. 1. The two mode formations on a two-dimensional structure of a ring that mimic the helical edge state of (a) the clockwise rotation and (b) the counterclockwise rotation with static magnetic fields toward the front of the paper and toward the back of the paper respectively, and (c) stacking pattern of two-dimensional periodic structure of rings with multiple surface modes.

flowing in the conductor structure and the potential difference generated between the structures is called the circuit theory.

Next, the principles of surface wave generation on the domino-ring structure are described. As shown in Fig. 2(a), the domino structures are placed through the interior of the ring structure. And the domino and ring structures generate surface wave modes based on the principles of wave theory and circuit theory, respectively. As shown in Fig. 2(b), in the domino structure, the electric field distribution is formed by the boundary conditions. In the ring structure shown in in Fig. 2(c), the voltage formed between the ring and the reference potential (GND) of the domino structure and the current in the ring are formed. Figure 2(d) shows that in coupling mode, an electric field distribution is formed between the reference potential of the domino structure and the ring structure. Surface modes excited by domino structures depend on the size of the unit cell and are generally on the subwavelength order. On the other hand, surface modes excited by ring structures depend on the circuit constants of the unit cell and include regions outside the subwavelength range. Coupling modes also depend on ring structures and thus include regions outside the subwavelength range.

Assuming that the conductive part of the domino structure is a perfect conductor, first the effective medium parameters

can be obtained by calculating the propagation mode and energy flow rate in the unit cell. Next, the dispersion relation can be derived by applying the resonance condition to the reflection coefficient at the boundary between the free space and the structure to find the singularity [44],

$$k = \frac{\omega}{c}\sqrt{\left(1 - \frac{a}{d}\right)^2 \tan\left(\frac{\pi}{2}\frac{\omega}{\omega_D}\right) + 1},$$

$$\omega_D = \frac{\pi c}{2h}. \tag{1}$$

Here, c, k, and ω are the velocity of light, a wavenumber, and an angular frequency, respectively. And a and d are the width and the arrangement period of the domino. ω_D is the cut-off angular frequency of the domino structure. As can be seen from Eq. (1), the contribution of the height h of the domino structure to the dispersion relation is relatively larger than the other parameters. In other words, in the domino structure, the electric field distribution forms a dominant mode in the vertical direction rather than in the arrangement direction. Figure 3 compares the dependence of ω/ω_D given by Eq. (1) on a/d and on height h. Figures 3(a) and 3(b) show the dependencies on a/d, and on height h, respectively. Comparing the results of Figs. 3(a) and 3(b), it can be seen that the change in the
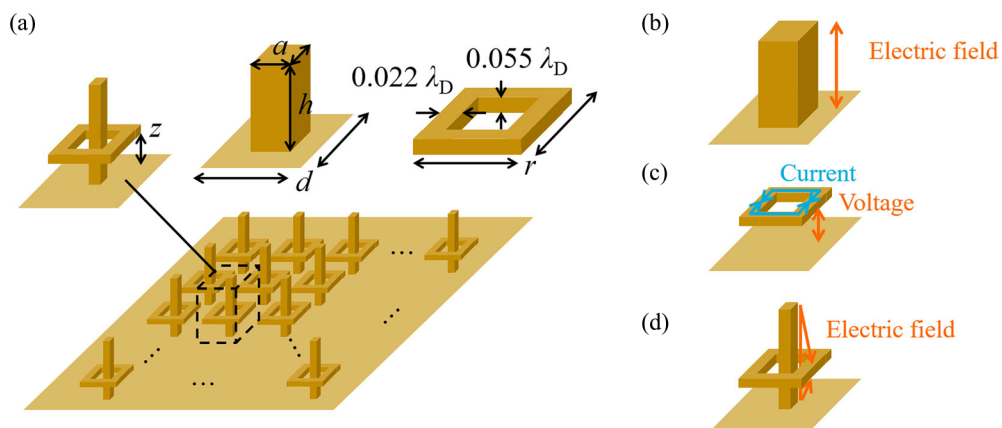

FIG. 2. (a) Schematic of domino-ring structure, and mode formations on the unit cell in the case of (b) domino, (c) ring, and (d) coupling mode. Here, λ_D is a wavelength in free space at the cut-off frequency of the domino structure.
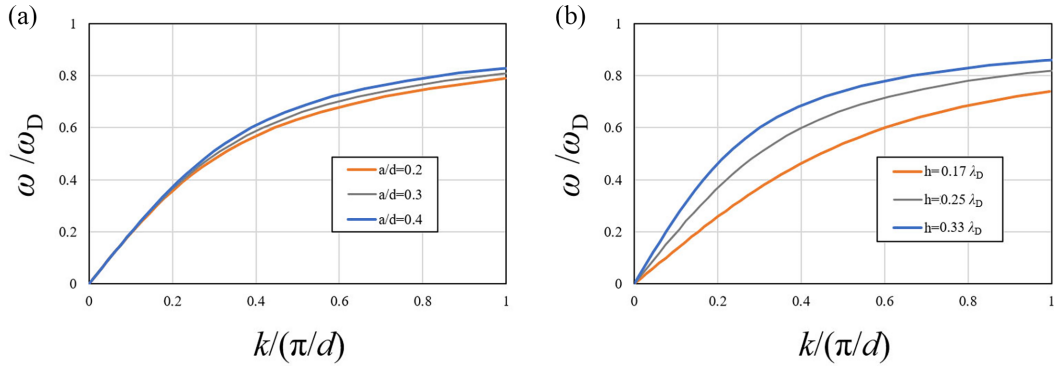
FIG. 3. Dispersion relations of domino structures in the cases of varying (a) a/d and (b) h.

dispersion relation is greater for h than for a/d with respect to the rate of change of values. This property can be used to generate a new mode with little effect on the dispersion relation of the domino structure, even if the ring structures are added.

On the other hand, it can be interpreted like that the ring structure forms a periodic transmission line to the propagation direction. Therefore, first the dispersion relation of the ring structure is obtained as follows, by deriving the characteristic impedance of the periodic transmission line [45,46]:

$$\cosh(\mathrm{i}kd) = 1 + Z(\omega)Y(\omega). \tag{2}$$

Here, $Z(\omega)$ and $Y(\omega)$ are an impedance and an admittance of the equivalent circuit model shown in Fig. 4(a), respectively. And these functions can also be expressed as, using circuit constants,

$$Z(\omega) = \mathrm{i}\left(\omega L - \frac{1}{\omega C'}\right),$$
$$Y(\omega) = \mathrm{i}\omega C, \tag{3}$$

where L is the inductance of the ring structure, C is the capacitance between rings and the reference potential, and C' is the capacitance between the ring structures. Therefore using these values, Eq. (2) can be replaced as

$$\cos(kd) = \left(1 + \frac{C}{C'}\right)\left[1 - \left(\frac{\omega}{\omega_{\mathrm{R}}}\right)^2\right]. \tag{4}$$
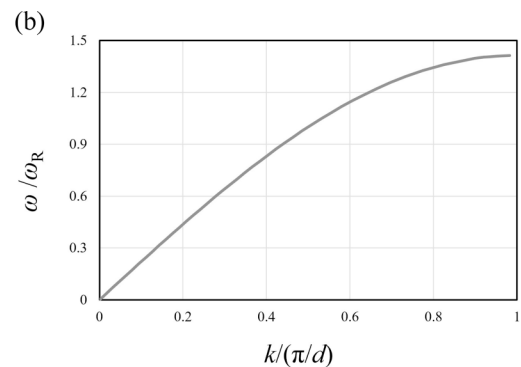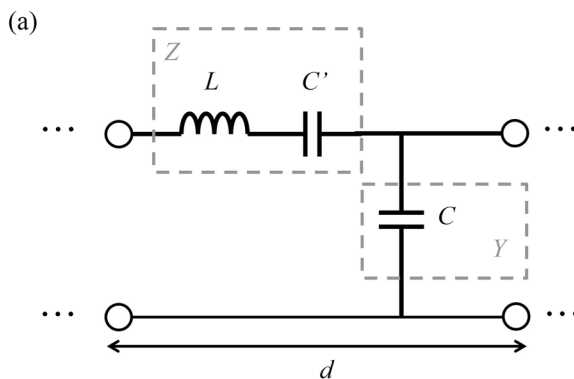
The cut-off angular frequency of the ring structure ω_{R} in Eq. (4) can also expressed as, using the circuit constants of L, C, and C',

$$\omega_{\mathrm{R}} = \sqrt{\frac{C + C'}{LCC'}}. \tag{5}$$

Since the capacitance between the ring structures is assumed to be sufficiently larger than the capacitance between the ring structure and the reference potential, Eqs. (4) and (5) can be approximated as follows, assuming that $C' \gg C$,

$$\cos(kd) \simeq 1 - \left(\frac{\omega}{\omega_{\mathrm{R}}}\right)^2, \tag{6}$$

$$\omega_{\mathrm{R}} \simeq \sqrt{\frac{1}{LC}}. \tag{7}$$

The graph of Eq. (6) is shown in Fig. 4(b). since it is difficult to derive L and C directly of the ring structure, the theoretical curve is fitted using the eigenmode frequency obtained from the analysis of the ring structure alone, and is used for comparison with the analysis results for the domino-ring structure. Finally, formation of coupling modes are explained. Propagation modes are created by the electric field distribution generated between the domino structure, which serves as the reference potential, and the ring structure, which has a constant potential. Thus, the number of coupling modes corresponds to the number of rings in the unit cell. The difference from the ring-derived mode is that the mode is generated from the boundary between the domino and the ring structure as a potential surface, and is not a mode created by the current

FIG. 4. (a) Equivalent circuit model and (b) dispersion relation of ring structure.

TABLE I. The structural parameters of a domino-ring structure as a reference model.

Parameter	d	a	h	r	z
Value	$0.25\lambda_D$	$0.089\lambda_D$	$0.25\lambda_D$	$0.22\lambda_D$	$0.056\lambda_D$

flowing in the ring. The difference from the domino-derived mode is that ring structures are also included as boundaries used for mode formation.

The coupling mode is useful for fine-tuning and tuning the frequency band without changing the structure because the cut-off angular frequency can be changed by moving the ring up and down. When the number of frequency bands used for sensing is to be increased, bands can be added by moving them within the target frequency band. For example, in bio/chemical sensing, the information obtained depends on the bandwidth, which can be advanced by shifting or increasing the bandwidth. When applied in the optical domain, as in the above example, the light lines are coupled at the bottom of the light line using a prism, or the backside of the light line is used for coupling. In the radio domain, the lattice scattering effect of the periodic structure is used to couple them in free space [13].

III. RESULTS AND DISCUSSIONS

Eigenvalue analysis was performed using an electromagnetic simulator (HFSS, 2020 R2) to verify the proposed method for generating and controlling multiple modes of surface waves using the domino-ring structure. First, the generation of multiple modes was confirmed by comparing the analytical results of dispersion relations for domino, ring,

and domino-ring structures with the theoretical curve for the domino structure and the fitting curve for the ring structure. In the domino-ring structure, the dispersion relations of the domino- and ring-derived modes obtained by the analyses are compared to the theoretical and fitting curves, respectively. Next, the controllability of the domino-derived mode and the ring-derived mode in the domino-ring structure was validated by comparing the analytical results of the structural parameter dependencies with the theoretical curves of the domino structures and the fitting curves of the ring structures. The reference dimensions of the structural parameters for the domino-ring structures are set as shown in Table I. Here, as shown in Fig. 2, r is the length of one side of ring and z is the position of ring.

The results of the comparison of the dispersion relations for the domino, ring, and domino-ring structures are shown in Fig. 5. In the following comparison with the analytical results, the results originated from the domino structure use the theoretical dispersion relation curve in Eq. (1), and the results originated from the ring structure use the fitting curve in Eq. (6) to the analytical results for the stand-alone case. Figures 5(a)–5(c) show that the domino structure has an eigenmode frequency of approximately $0.78\ \omega_D$ and size of 1/5 wavelength or less, while the ring structure has an eigenmode frequency of approximately $1.2\ \omega_D$ and size of 1/3 wavelength or less. For the domino and ring structures, respectively, the analytical results are in good agreement with the theoretical and fitting curves, and especially for the domino-structure mode, the error between the theoretical curve and the analytical results is less than 3.7 percent. The dispersion relation of the domino-ring structures shows that the characteristics of each structure are maintained. In addition, a new mode that is not consistent with the domino and ring structures has been identified, and this mode is referred to as the coupling mode. This mode is considered to be formed between
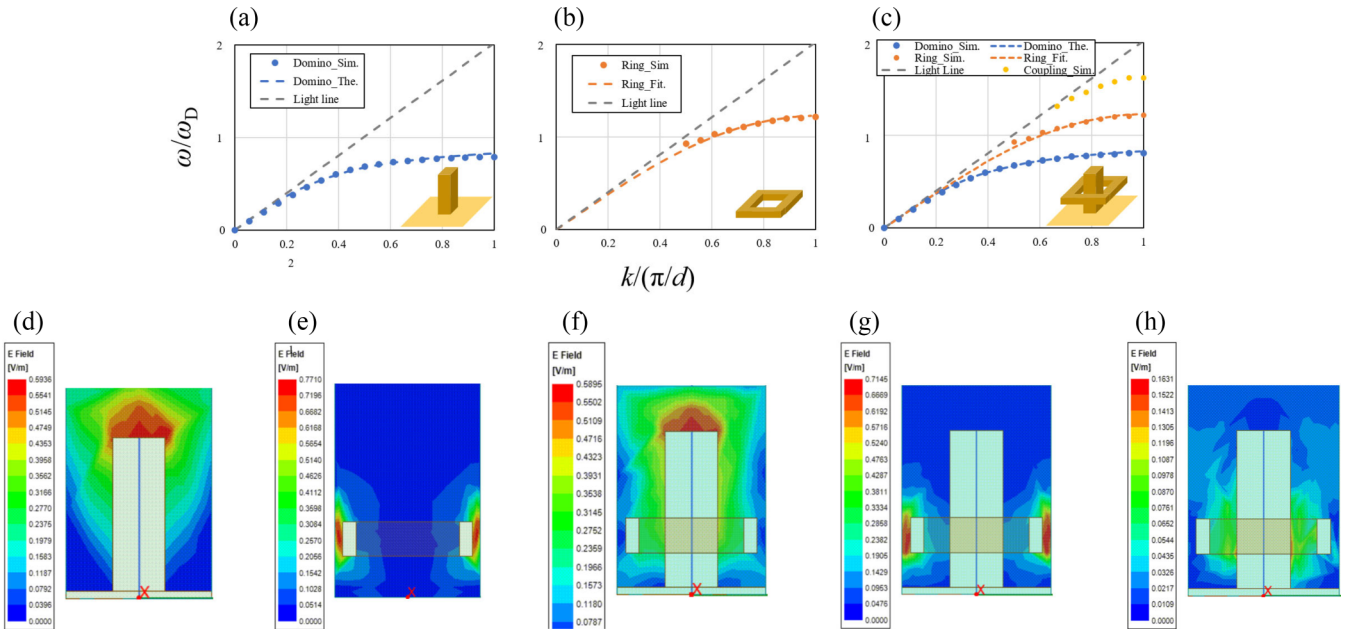

FIG. 5. Comparison results of dispersion relation between (a) domino, (b) ring, and (c) domino-ring structures. Electric distributions of (d) domino, (e) ring, and (f)–(h) domino-ring structures at each eigenmode frequencies of (d) $0.75\ \omega_D$, (e) $1.18\ \omega_D$, (f) $0.78\ \omega_D$ (corresponding to the domino mode), (g) $1.2\ \omega_D$ (corresponding to the ring mode), (h) $1.64\ \omega_D$ (corresponding to the coupling mode).
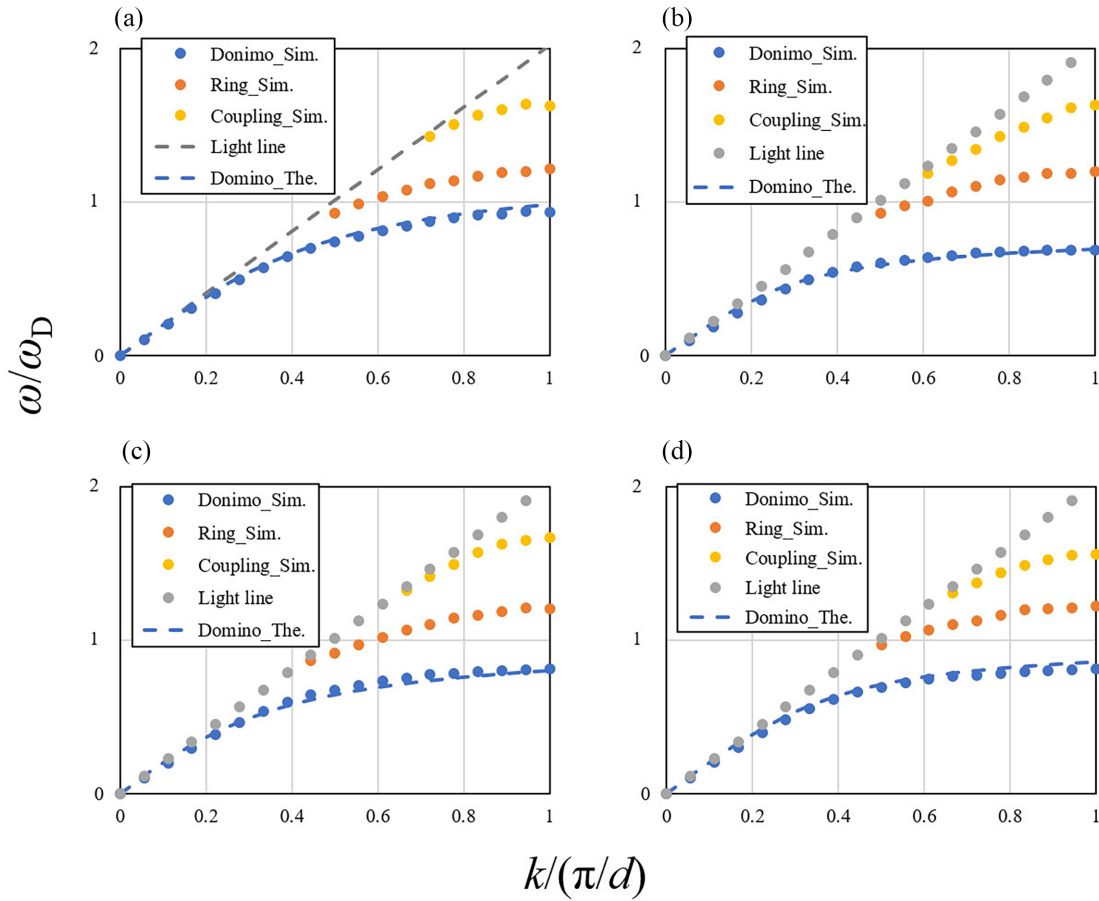
FIG. 6. h and a/d dependencies of dispersion relation of domino-ring structure. (a) $h = 0.2\lambda_D$ smaller than that of the reference model, (b) $h = 0.31\lambda_D$ larger than that of the reference model, (c) $a/d = 0.22$ smaller than that of the reference model, (d) $a/d = 0.49$ larger than that of the reference model.

the domino and ring structures. Figures 5(d)–5(h) show the electric field distributions at the eigenmode frequencies of the domino structure, the ring structure, and the first to third modes of the domino-ring structure, respectively. From the results of Figs. 5(d) and 5(f), the first mode of the domino-ring structure behaves similarly to the electric field distribution of the mode of the domino structure, confirming that the first mode is derived from the domino structure. Similarly, from the results of Figs. 5(e) and 5(g), the behavior of the second mode of the domino-ring structure is similar to the electric field distribution of the mode of the ring structure, and it confirmed that the second mode is derived from the ring structure. Figure 5(h) shows the electric field distribution of the third mode. The third mode is considered to be a coupling mode because the distribution spreads between the ring and domino structures. On the other hand, the third mode has smaller wavenumbers at the eigenmode frequencies of the domino (0.78 ω_D) and ring modes (1.18 ω_D), so it can be judged to be a different mode from domino and ring modes when compared to the distributions of Figs. 5(d) and 5(e).

Next, the structural parameter dependencies of each modes in the domino-ring structure are described. Based on the reference model shown in Table I, the results of the dispersion relations are compared when each structural parameter is varied. Note that the dispersion curves of the reference model shown in Table I are in Fig. 5(c). Figures 6(a) and

6(b) compare the dispersion curves for different heights of domino h, in the domino-ring structure. The analytical results of the domino-derived modes and the corresponding theoretical curves show good agreement, with an error of less than 5.8 percent. It can also be confirmed that there is a shift to the low frequency side as the height h increases from (a) to (b). This result is consistent with the fact that the cut-off frequency ω_D expressed in Eq. (1) is inversely proportional to the height h. And the other modes are almost unvaried when changing h. Similarly, Figs. 6(c) and 6(d) compare the dispersion curves when a/d is varied. Here, d was kept constant and only the width of domino a, was varied. The theoretical curve is consistent with the analytical results, with an error of less than 5.6 percent. It can also be seen that the analytical results of the domino- and ring-derived modes are almost unvaried and the coupling mode is shifted to the lower frequency band as a/d increases from (c) to (d). In Fig. 6, the results indicate that the dispersion curve of the ring-derived mode are almost unchanged when h and a/d are varied, and that the dispersion curves of the domino-derived modes and the coupling modes can be controlled independently by changing h and a/d, respectively.

Figures 7(a) and 7(b) show the change in the dispersion curves of the domino-ring structure for different values of r. The analytical results of the ring-derived modes are in good agreement with the corresponding fitting curves; a shift
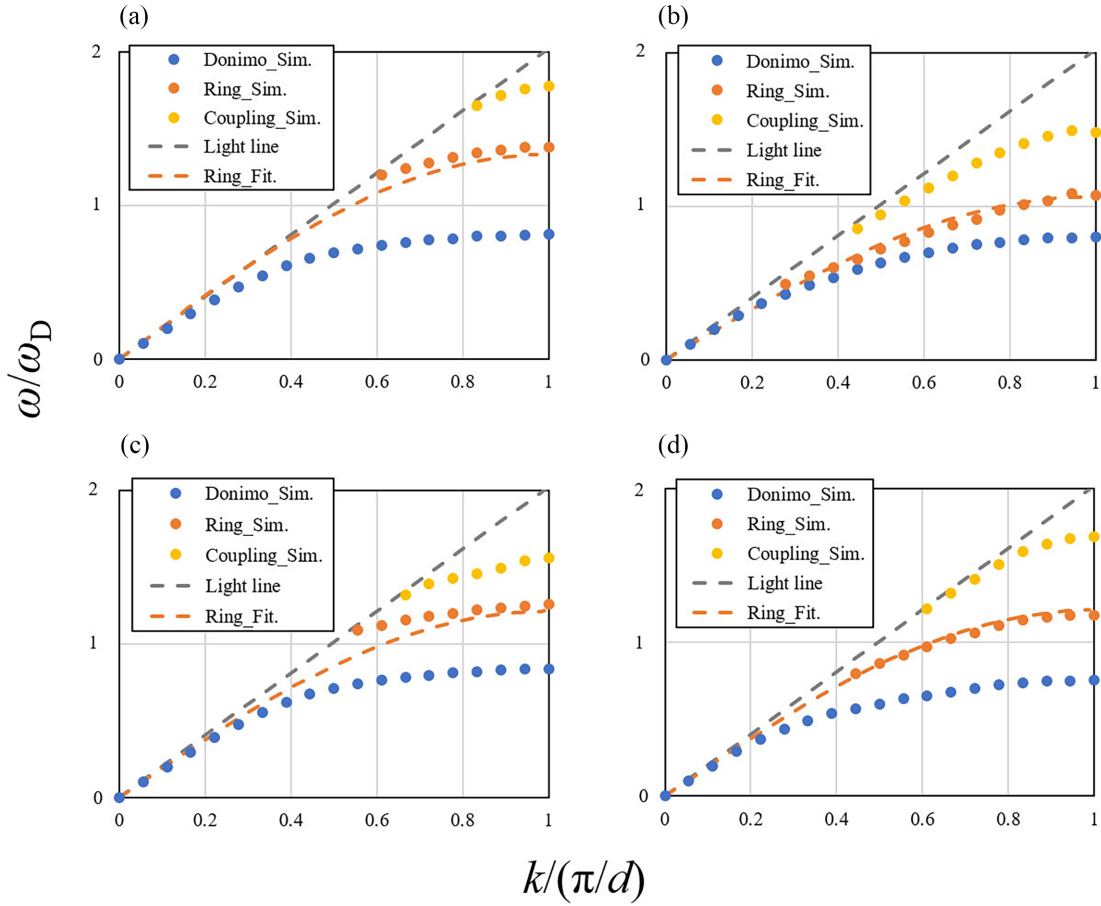
FIG. 7. r and z dependencies of dispersion relation of domino-ring structure. (a) $r = 0.2\lambda_D$ smaller than that of the reference model, (b) $r = 0.24\lambda_D$ larger than that of the reference model, (c) $z = 0.022\lambda_D$ smaller than that of the reference model, (d) $z = 0.11\lambda_D$ larger than that of the reference model.

to the low-frequency side as r increases from (a) to (b) is also reproduced. The analytical results of the domino-derived modes remains almost unchanged, while the analytical results of the coupling mode show a frequency shift in conjunction with the results of the ring-derived modes. In other words, the susceptibility of the coupling mode to changes in the structural parameters of the ring in the domino-ring structure is confirmed. Similarly, Figs. 7(c) and 7(d) show the change in dispersion curves when the position z of the ring structure is changed. Both the fitting curve and the analytical results for the ring-derived modes are almost unchanged, and the analytical results of the domino-derived mode and the coupling mode are changed when z is increased from (c) to (d). Therefore, it can be seen that the relative positional relationship between the domino and ring structures affects the coupling mode. From the above, it indicates that the frequency band of the coupling mode can be controlled by changing the position of the ring structure although the domino-derived mode is also changed. The ring-derived mode is almost independent of the position, suggesting that the cut-off angular frequency ω_R is dominated by the inductance L of the ring structure. The fact is also consistent with the design concept since the mode operation of the ring structure is assumed to be closed within a two-dimensional system.

From the above discussions, it confirmed that the domino- and ring- derived modes in the domino-ring structure can be

independently controlled by changing the height h, and one side r and the position z. The coupling mode can be controlled independently by changing the position a/d. The anaylytical results of the domino- and ring-derived modes in the domino-ring structure are in good agreement with the results of the dispersion curves of the domino and ring structures respectively, suggesting that the entire design is not necessary and can be easily handled by the individual designs. The features of the structural parameter dependencies of the dispersion relations on the domino-ring structure are summarized as Table II.

Finally, Fig. 8 shows the results of varying the number of ring structures. However, all of the ring structures have different positions, and three patterns are used: $z_1 = 0.011\lambda_D$,

TABLE II. The features of the structural parameter dependencies of the dispersion relations on the domino-ring structure.

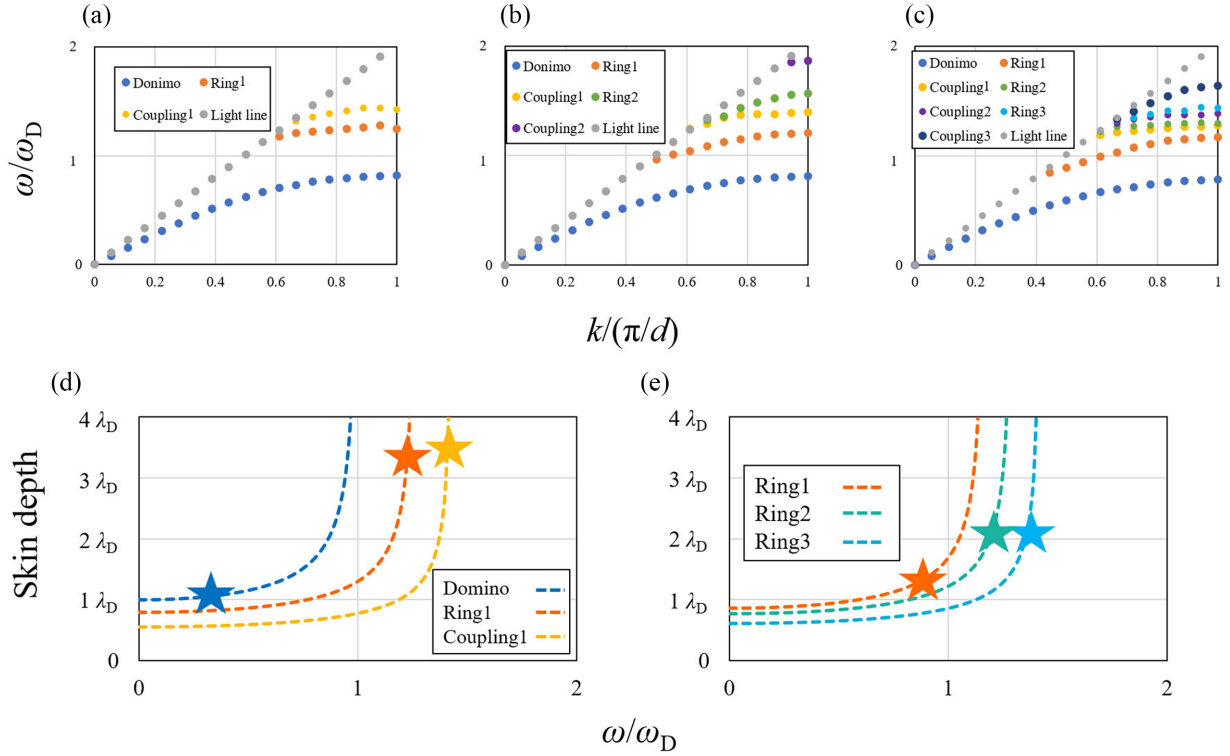|		Type of mode		
		Domino	Ring	Coupling
Structural parameter	h	Varied	Unvaried	Unvaried
	a/d	Unvaried	Unvaried	Varied
	r	Unvaried	Varied	Varied
	z	Varied	Unvaried	Varied

FIG. 8. Number-of-ring dependency of dispersion relation of the domino-ring structure. (a) The case of one ring at $z = z_1$, (b) the case of two rings at $z = z_1$ and z_2, (c) the case of three rings at $z = z_1$, z_2 and z_3. Skin depth characteristics of the surface modes of domino, ring, and coupling modes in the cases of (d) the result of (a) with the condition when coupled with evanescent waves using prisms with refractive index of 1.35 and (e) the result of (c) with the condition of refractive index of 1.1.

$z_2 = 0.089\lambda_D$, and $z_3 = 0.17\lambda_D$. Although the size of the rings are the same as the domino-ring structure shown in Table I, in Figs. 8(a)–8(c), the domino-derived mode and each ring-derived mode, and coupling modes formed between each ring structure and the domino structure were confirmed. The number of modes is three for one ring structure in (a), five for two ring structures in (b), and seven for three ring structures in (c). These results indicate that new modes can be generated by adding rings of different positions, and that as many coupling modes are generated as the number of rings. The correspondence between the ring-derived/coupling modes and the number of ring structures with different geometries is consistent with the design concept of domino-ring structures described in the previous section. The domino-ring structure can be considered to mimic a topological material as a two-dimensional electronic material, suggesting that each structure can be stacked independently. It is also found that the surface modes can be multiplexed following to the design principle. In this verification, the number of rings is limited to a maximum of three, but the number of multiple modes can be further increased by optimizing the size and shape of the rings.

Figures 8(d) and 8(e) show the results of calculating the skin depth of each mode for the structures showing dispersion curves in (a) and (c) respectively, assuming that the modes are coupled with evanescent waves using prisms with refractive indices of 1.35 and 1.1 [33–36]. Note that in (e), the cases domino and coupling modes are omitted. From (d), the skin depths for the domino mode, ring mode, and coupling mode

are $1.1\lambda_D$, $3.6\lambda_D$, and $3.8\lambda_D$, respectively. Since the skin depth differs depending on the mode, it is considered that the depth information can be derived by combining the sensing information obtained from each mode. From (e), the respective skin depths of the modes in each ring are $1.4~\lambda_D$, $2.1~\lambda_D$, and $2.1~\lambda_D$, respectively. It can be seen that the skin depths of Ring 2 and Ring 3 modes are almost equal. Therefore, there is a possibility that two-dimensional information on a specific depth position can be obtained with high accuracy or high resolution in multiple bandwidths. Thus the two results suggest that the incident waves of multiple bandwidths may simultaneously excite surface modes in multiple bandwidths, increasing the wavelength information of sensing and improving spatial resolution, and open up the possibility of improving the communication and sensing technologies such as optical- and radio frequency waveguides, bio/chemical sensing, and biomedical diagnosis.

IV. CONCLUSIONS

In this study, a design method for generating and controlling multiple surface wave modes by using the domino-ring structure is proposed. This method is based on the combination of a domino structure, which is a typical structure for surface wave generation, and multiple ring structures. The design is based on the concept of mimicking the physical properties of topological material such as helical edge state and Chern number by using the two-dimensional periodic structures of the ring and stacking the structures for mul-

tiplexing the modes. The domino structure, which forms a waveguide, gives a reference potential to the ring structures to realize a waveguide that forms multiple modes. In order to verify the proposed method, first the generation of multiple modes was confirmed by comparing the analytical results of the dispersion relations for the domino structure, ring structure, and domino-ring structure with the theoretical curve for the domino structure and the fitting curve for the ring structure. Next, the controllability of surface wave modes originating from the domino and ring structures in the domino-ring structure was validated by comparing the analytical results of the structural parameter dependencies with the theoretical curves of the domino structures and the fitting curves of the ring structures.

The results confirmed the possibility of generation of multiple modes in the domino-ring structure. And the domino- and ring-derived modes showed good agreement with the theoretical curve of the domino structure and the fitting curve of the ring structure, respectively. The domino-derived mode showed a maximum error of 5.8 percent compared with the theoretical curve.

It is also confirmed that the domino- and ring-derived modes in the domino-ring structure can be independently controlled by changing the height h, and one side r and the position z. Also, the coupling mode can be controlled independently by changing the size ratio of a/d. The dispersion curves of the domino- and ring-derived modes in the domino-ring structure are in good agreement with the results of the dispersion curves in the case of the domino and ring structure respectively, suggesting that the entire design is not needed and can be easily handled by individual design. And, the results indicated that new modes can be generated by adding rings of different positions and sizes in the unit cell, and that as many coupling modes are generated as the number of rings. Finally, the skin depth of multiple surface modes on the domino-ring structure was calculated under the assumption that the modes are coupled with evanescent waves using prisms with refractive indices of 1.35 and 1.1. The results indicated the possibility of increasing the wavelength information and improving spatial resolution if using multiple surface modes.

[1] J. Heckmann, K. Pufahl, P. Franz, N. B. Grosse, X. Li, and U. Woggon, Phys. Rev. B **98**, 115415 (2018).

[2] C.-Y. Wang, H.-Y. Chen, L. Sun, W.-L. Chen, Y.-M. Chang, H. Ahn, X. Li, and S. Gwo, Nat. Commun. **6**, 7734 (2015).

[3] I. Antohe, I. Iordache, V.-A. Antohe, and G. Socol, Sci. Rep. **11**, 10086 (2021).

[4] A. P. Vinogradov, A. V. Dorofeenko, A. A. Pukhov, and A. A. Lisyansky, Phys. Rev. B **97**, 235407 (2018).

[5] L. Wang, L.-G. Wang, L.-H. Ye, M. Al-Amri, S.-Y. Zhu, and M. S. Zubairy, Phys. Rev. A **94**, 013806 (2016).

[6] S. Thongrattanasiri and F. J. G. de Abajo, Phys. Rev. Lett. **110**, 187401 (2013).

[7] H. G. Frey, S. Witt, K. Felderer, and R. Guckenberger, Phys. Rev. Lett. **93**, 200801 (2004).

[8] P. D. Lacharmoise, N. G. Tognalli, A. R. Goni, M. I. Alonso, A. Fainstein, R. M. Cole, J. J. Baumberg, J. Garciade de Abajo, and P. N. Bartlett, Phys. Rev. B **78**, 125410 (2008).

[9] B. Vasić and R. Gajić, Phys. Rev. Appl. **4**, 024007 (2015).

[10] Y. Luan, L. McDermott, F. Hu, and Z. Fei, Phys. Rev. Appl. **13**, 034020 (2020).

[11] T. W. Ebbesen, H. J. Lezec, H. F. Ghaemi, T. Thio, and P. A. Wolff, Nature (London) **391**, 667 (1998).

[12] J. B. Pendry, L. M.- Moreno, F. J. G.- Vidal, Science **305**, 847 (2004).

[13] F. J. Garcia-Vidal, L. Martin-Moreno, T. W. Ebbesen, and L. Kuipers, Rev. Mod. Phys. **82**, 729 (2010).

[14] Y. Tokizane, S. Ohno, Y. Takida, J.-I. Shikata, and H. Minamide, Phys. Rev. Appl. **17**, 054020 (2022).

[15] F. Miyamaru and M. Hangyo, Phys. Rev. B **72**, 035429 (2005).

[16] J. B. Pendry, Phys. Rev. Lett. **85**, 3966 (2000).

[17] R. A. Shelby, D. R. Smith, and S. Schultz, Science **292**, 77 (2001).

[18] F. Falcone, T. Lopetegi, M. A. G. Laso, J. D. Baena, J. Bonache, M. Beruete, R. Marqués, F. Martín, and M. Sorolla, Phys. Rev. Lett. **93**, 197401 (2004).

[19] G. Itami and O. Sakai, Sci. Rep. **10**, 11027 (2020).

[20] Y. Pang, Y. Li, J. Zhang, Z. Xu, and S. Qu, IEEE Microw. Wirel. Propag. Lett. **17**, 1123 (2018).

[21] H. C. Zhang, P. H. He, X. Gao, W. X. Tang, and T. J. Cui, J. Phys.: Condens. Matter **30**, 134004 (2018).

[22] A. Kandwal, Q. Zhang, X.-L. Tang, L. W. Liu, and G. Zhang, IEEE Microw. Wirel. Propag. Lett. **17**, 184 (2018).

[23] Z. Ma, S. M. Hanham, P. A. Huidobro, Y. Gong, M. Hong, N. Klein, and S. A. Maier, APL Photonics **2**, 116102 (2017).

[24] K. v. Klitzing, G. Dorda, and M. Pepper, Phys. Rev. Lett. **45**, 494 (1980).

[25] D. J. Thouless, M. Kohmoto, M. P. Nightingale, and M. den Nijs, Phys. Rev. Lett. **49**, 405 (1982).

[26] Y. Hatsugai, Phys. Rev. Lett. **71**, 3697 (1993).

[27] B. A. Bernevig, and S.-C. Zhang, Phys. Rev. Lett. **96**, 106802 (2006).

[28] M. König, S. Wiedmann, C. Brüne, A. Roth, H. Buhmann, L. Molenkamp, X.-L. Qi, and S.-C. Zhang, Science **318**, 766 (2007).

[29] A. Roth, C. Brüne, H. Buhmann, L. W. Molenkamp, J. Maciejko, X.-L. Qi, and S.-C. Zhang, Science **325**, 294 (2009).

[30] K.-I. Sasaki, Phys. Rev. B **105**, 075312 (2022).

[31] B. Stein, J.-Y. Laluet, E. Devaux, C. Genet, and T. W. Ebbesen, Phys. Rev. Lett. **105**, 266804 (2010).

[32] Z. Xu, Y. Wang, J. Chang, and T. J. Cui, Phys. Rev. Appl. **18**, 024035 (2022).

[33] S. Jahani and Z. Jacob, Nat. Nanotechnol. **11**, 23 (2016).

[34] F. Miyamaru, M. Tanaka, and M. Hangyo, Phys. Rev. B **74**, 153416 (2006).

[35] O. Schnitzer, Phys. Rev. B **96**, 085424 (2017).

[36] G. Itami and O. Sakai, J. Appl. Phys. **125**, 213101 (2019).

[37] G. Itami, O. Sakai, and Y. Harada, Electronics **8**, 239 (2019).

[38] G. Liu, D. Cheng, B. Zhang, G. Shu, and J. Wang, J. Phys. D: Appl. Phys. **52**, 205401 (2019).

[39] G. R. Muns, K. V. Mishra, C. B. Guerra, Y. C. Eldar, and K. R. Chowdhury, *in IEEE International Conference on Computer Communications* (IEEE INFOCOM, April 2019), p. 535.

[40] A. Ali, N. G.- Prelcic, and A. Ghosh, IEEE Trans. Veh. Technol. **69**, 14903 (2020).

[41] M. A. K. Othman, V. A. Tamma, and F. Capolino, IEEE Trans. Plasma Sci. **44**, 594 (2016).

[42] A. I. Fernández-Domínguez, E. Moreno, L. Martín-Moreno, and F. J. Garcia-Vidal, Phys. Rev. B **79**, 233104 (2009).

[43] S. Anuthum, F. Hasegawa, C. Lertvachirapaiboon, K. Shinbo, K. Kato, K. Ounnunkad, and A. Baba, Phys. Chem. Chem. Phys. **24**, 7060 (2022).

[44] F. J. Garcia-Vidal, L. M. Moreno, and J. B. Pendry, J. Opt. A: Pure Appl. Opt. **7**, S97 (2005).

[45] A. Sanada, C. Caloz, and T. Itoh, IEEE Microw. Wirel. Compon. Lett. **14**, 68 (2004).

[46] S. Nagai and A. Sanada, IEICE Electron. Expr. **13**, 20160281 (2016).